applied sciences

MDPI

Article

An Independent Internal Cooling System for Promoting Heat Dissipation during Dry Cutting with Numerical and Experimental Verification

Bin Yao [1], Weifang Sun [1], Binqiang Chen [1,*], Xiaojin Yu [1], Yuchao He [1], Wei Feng [2] and Shuyang Wang [1]

[1] School of Aerospace Engineering, Xiamen University, Xiamen 361005, Fujian, China; Yaobin@xmu.edu.cn (B.Y.); Vincent_suen@126.com (W.S.); yuxiao084@163.com (X.Y.); heyuchao1993@126.com (Y.H.); xmuwsy@126.com (S.W.)

[2] School of Mechanical and Electrical Engineering, Henan University of Technology, Zhengzhou 450007, Henan, China; skyseacloud2006@126.com

* Correspondence: cbq@xmu.edu.cn; Tel.: +86-592-2186-383

Academic Editor: Yulong Ding
Received: 26 December 2016; Accepted: 23 March 2017; Published: 28 March 2017

Abstract: The cooling system has emerged as an effective way to alleviate the excessive heat generation during dry cutting processes. In this paper, we investigated a novel type of internal cooling system, independent of additional mechanical accessories, as a promising cooling alternative. The proposed system is devised as connected internal fluid channels of a-"V" shape created according to the geometric shape of the tool-holder. Enabling quantitative evaluation of the effectiveness of the proposed system, a new numerical approach is established. Within the approach, heat transfer equations are deduced according to thermodynamics; parameters of the equations are specified via analytical modeling. As a result, cutting temperatures can be estimated with high precision according to the outlet temperature. Moreover, a cutting experiment was carried out to verify the effectiveness of the proposed numerical approach. Tool-chip interface temperatures were measured using an infrared thermal imager. Smooth measurements with suppressed noises are derived based on a new adaptive mean filter originated by empirical mode decomposition (EMD). The experimental results demonstrate the proposed system can reduce the temperature substantially (almost 30% at the measuring point) and the results are highly consistent with those of numerical simulation. The proposed cooling system is a prospective enhancement for development of smart cutting tools.

Keywords: indirect cooling systems (ICS); internal fluid channel; dry cutting; enhanced heat transfer

1. Introduction

An excessiverise in temperature due to heat generation during the cutting process is an important issue that not only accelerates tool wear but also affects machining accuracy and surface quality of the finished workpieces [1]. Therefore, the research on active control of cutting temperature via promotion of heat-dissipation is indispensable for a highly reliable machining process. Wet machining using different kinds of cutting fluids is a most widely used technique to maintain the cutting temperature below some specified optimal cutting temperatures [2]. However, the excessive use of cutting fluids becomes a major problem owing to some associated economic, environmental and health concerns [3]. Dry machining can be considered as a feasible approach to eliminate the use of cutting fluids because of low processing cost and soft ecological hazard [4]. Compared with wet machining, dry cutting shows some superiority such as lower thermal shock and improved useful life of cutting tools, however, the machining friction and the cutting temperature during dry machining are usually greater than

those of wet machining. Temperature has an impact on tool wear, thus it is important for the cutting process [5,6]. Aiming at achieving better temperature reduction performance in dry machining process, researchers have proposed a variety of methods and achieved some meaningful results. Jerold [7] and Tazehkand [8] investigated the utilization of CO_2 and liquid nitrogen as cooling media to reduce the cutting temperature and reported good improvements. On the other hand, heat pipe cooling is also a widely utilized method to improve cutting performances and has attracted significant attentions [9,10].

Regarded as an indirect cooling system (ICS), research on the internal cooling system has already been a hot topic in industry because of its convenient installation for conventional machine tools. Since the initial description of this type of cooling system in the 1970s, a variety of improvements have been proposed. Ferri designed an internally cooled cutting tool consisting of a modified cutting insert, cooling adapter accommodating micro-channel, and tool-holder with inlet and outlet ports [11]. Minton created a modified tool-holder with an internally cooled tool to enhance the heat transfer [12]. In these two studies, pyrometers were employed to monitor the rise of cutting temperature and evaluate the enhancement of cooling effect. Sun presented an enclosed internal cooling circuit in the support seat [13], and in his study, a thermal imager was employed to measure cutting temperatures in the machining process. Among the above reported literature, research on ICS mainly focuses on modifications of tool-holder forms, support seat or the insert. These methods above can indeed be improved, however they usually require additional supply devices that inevitably increase the complexity of the machining tool or modify the machine tool structure, significantly limiting industrial applications.

Considering the pros and cons of the above cooling methods, in this paper, a novel independent cooling system based on an internal cooling fluid channel is devised and applied to promote heat dissipation during cutting process. A distinct advantage of this novel ICS lies in its simplified mechanical structure and high heat dissipation-promoting performance. Compared with traditional ICS, the proposed independent internal cooling system needs only limited modification for the cutting component and the cooling media can also be replaced by the existing refrigerating system. The heat–energy balance equations of the cooling structure are established to evaluate the cutting temperature. Temperature fields on the rake face and on the flank face were simulated on the numerical platform of Ansys CFX (12.1, ANSYS, Inc., Canonsburg, PA, USA, 2009). Moreover, turning tests were carried out to verify the validation of the numerical model which was previously put forward. In the experiments, turning tests were performed on workpieces made of medium carbon steel of the grade 1045 (the carbon content in the steel is 0.45% according to technical standard provided by the American society for testing and materials). The experimental results demonstrated the effectiveness of the novel independent ICS and the improved cooling performance.

2. Design of Cutting Tool with Independent Internal Cooling Structure

The internal cooling cutting tool system, based on a novel internal channel and designed to enhance heat transfer, is presented in Figure 1. A carbide insert (YT14 (ISO P20) 31303C, Zhuzhou Cemented Carbide Cutting Tools, LTD, Zhuzhou, Hunan, China) was used in this research. A tool-holder (90° 20W3K13, Taizhou Tingfeng CNC Tools Co., LTD, Taizhou, Zhejiang, China) was modified with a connected V-shaped channel created inside. The cooling liquid was pumped with a peristaltic pump through the V-shaped channel and forming a closed internal cooling circuitry in the tool-holder. Three tiny grooves were machined by the electrospark wire-electrode for placing the thermocouples for temperature measurement. Three temperature measure points were marked with red circles in Figure 1a. V-shaped channel (colored part) and its design parameters are described in Figure 1b, different colors represented the temperature distribution in the CFX simulation process. The thermal flux from the machining process is conduced into the insert and then permeates into the air and the channel. The area of high values of thermal flux in the field is extremely localized because of the relatively small area of the tool-chip interface. Therefore, practical cooling channels of high performance are supposed to be placed around the insert rake face in a manner as closed as possible.

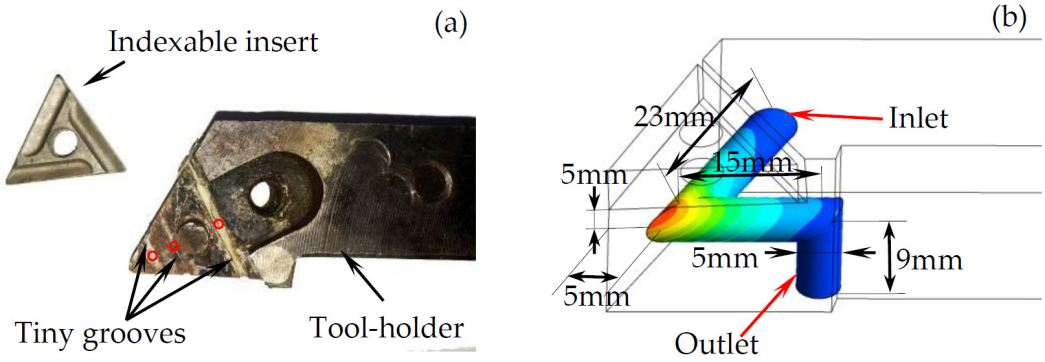

Figure 1. Schematic illustration of cutting tool assembly: (**a**) cutting tool; (**b**) the modified tool-holder with V-shaped channel.

3. Numerical Analysis of the Thermal Performance

Figure 2 illustrates the triangle indexable insert and the definition of the coordinate systems in this research. The variable L is the side length of the equilateral triangle; and the variable h is referred to as the thickness of the insert. The area marked by white rhombus in Figure 2a indicates the tool-chip interface in the machining process. Let w be the cutting width and a_p be the depth of cut. Therefore, the cutting area can be presented as $A_c \approx w \cdot a_p$. The tool-chip contact area is very small compared with the insert surface. Previous research showed that the maximum cutting temperature is located at a position that is near the center of the tool-chip contact area. For simplicity, the tool-chip contact face was assumed as a uniform temperature distribution area [14]. There are three different coordinate systems, which are defined as $S(XOY)$, $S_1(X_1O_1Y_1)$ and $S_2(X_2O_2Y_2)$. $S(XOY)$ is the coordinate system established on the rake face; $S_1(X_1O_1Y_1)$ denotes the main flank face of the insert; and $S_2(X_2O_2Y_2)$ stands for the minor flank face. The three distinct coordinate systems coincide at the same origin that is located at the tool tip.

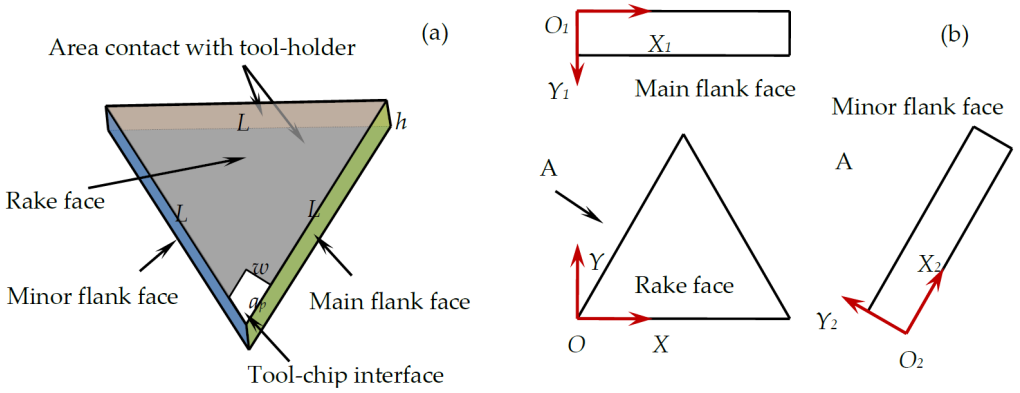

Figure 2. Schematic of the indexable insert: (**a**) surfaces definition and (**b**) coordinate systems definition.

3.1. Energy Balancing

The heat–energy balance equations of the insert system can be written as follows [14,15]:

$$\begin{cases} c_t \rho_t V_t \frac{dT_{insert}}{dt} = qA_c - q_r - q_{f1} - q_{f2} - q_{tl} - q_{th} \\ c_l \rho_l V_l \frac{dT_o}{dt} = q_{tl} \end{cases} \quad (1)$$

where all the physical meanings of the variables in Equation (1) are listed in Table 1.

Table 1. Physical meaning of the variables in Equation (1).

Variables	Meaning
c_t, ρ_t, V_t	the heat capacity, mass density, and volume of the insert
c_l, ρ_l, V_l	the heat capacity mass density and volume of the cooling liquid
T_{insert}	the averaged temperature of the insert
q	the heat flux on contact area
A_c	the area of the tool-chip contact surface
q_{rf}, q_{f_1}, q_{f_2}	the heat that dissipates into air through the rake face, the main flank face and the minor flank face, respectively
q_{tl}, q_{th}	the heat that conduct into the channel and the tool-holder, respectively
T_o	the temperature of outlet of the internal cooling channel

According to Newton's law of heat transfer, Equation (1) can be rewritten as below:

$$\begin{cases} c_t\rho_t V_t \frac{dT_{insert}}{dt} & = qA_c - \iint_{A_r - A_c} h(T_r(x,y,t) - T_{air})dA \\ & \quad - \iint_{A_{f1}} h(T_{f1}(x_1,y_1,t) - T_{air})dA \\ & \quad - \iint_{A_{f2}} h(T_{f2}(x_2,y_2,t) - T_{air})dA \\ & \quad - q_{tl} - q_{th} \\ c_l\rho_l V_l \frac{dT_o}{dt} & = q_{tl} \end{cases} \tag{2}$$

where h denotes the heat transfer coefficient of the area exposed to the air, and the quantities $T_r(x,y,t)$, $T_{f1}(x_1,y_1,t)$ and $T_{f2}(x_2,y_2,t)$ denote temperature of the rake face, the main flank face and the minor flank face, respectively.

As can be seen in the above, an essential problem of applying Equation (2) lies in that there are many unknown quantities (T_{insert}, T_r, T_{f1}, T_{f2}, q_{tl}, q_{th}) that are difficult to be determined. Values of these unknown quantities will be explained and specified explicitly in detail in the following sub-sections.

3.2. Approximation of the Temperature Fields

Calculating the temperature fields on the rake face, the main flank face and the minor flank face is indispensable for evaluating the quantity of heat that dissipates into the air. In this work, the temperature fields of these surfaces were obtained via a numerical simulation platform of Ansys CFX. In order to acquire the temperature field distribution, finite element orthogonal simulation is performed to acquire the relationship of cutting depth and contact area temperature when cooling liquid velocity was fixed in 80 mL/min. Assume that the generated heats in cutting process are all dissipated through chip, tool and workpiece. Select the working fluid as water. The interface between internal channel and tool-holder is set as the "Fluid–Solid Interface". The interface between insert and tool-holder is set as the "Solid–Solid Interface". The simulation parameters are listed in Table 2. Figure 3 illustrates the tool temperature contours at one experimental point. The contact area was set as 1.0 mm × 0.1 mm. The temperature on the contact area was 1000 °C. It can be inferred from Figure 3 that the maximum value and the greatest gradient of the temperature fields on the three surfaces occur simultaneously at the tool nose. In order to summarize the temperature field mathematically, fitting methods will be used in this study.

Table 2. Simulation parameters.

Parameters	Insert	Tool-Holder	Water
Density (g/cm^3)	15	7.85	1
Thermal conductivity (W/(m·°C))	46	60	0.6
Specific heat capacity (J/(kg·°C))	203	462	4200
Air temperature (°C)		20	
Water temperature (°C)		20	
Viscosity of water (kg/(m·s))		0.001	
Inlet velocity (mL/min)		80	
Heat transfer coefficient (W/(m^2·°C))		8	
Cutting width (mm)		0.1	
Cutting depth (mm)		0.02, 0.1, 0.2, 0.5	
Contact area temperature (°C)		100, 400, 700, 900, 1200	

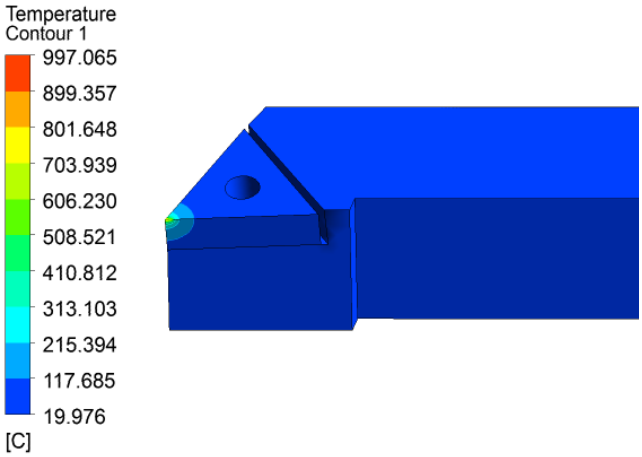

Figure 3. Temperature field with internal cooling structure created inside the tool-holder.

3.2.1. Temperature Filed on the Rake Face

Figure 4 shows the temperature field on the rake face, where different colors represented the temperature distribution in the CFX simulation process. To ensure proper fitting of the field, three straight line paths, which are denoted by $L1$, $L2$, $L3$, were deployed to probe the temperatures on them. The temperature distributions along the three straight lines are shown in Figure 5. Figure 5 shows their temperature distribution have little difference. Considering the characteristics of the temperature distributions, negative exponential function is suitable to illustrate it.

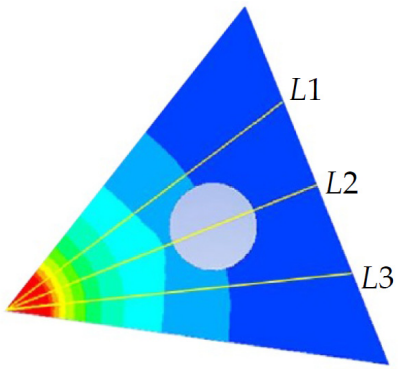

Figure 4. The simulated temperature field on the rake face. $L1$, $L2$, $L3$ denote three straight line paths.

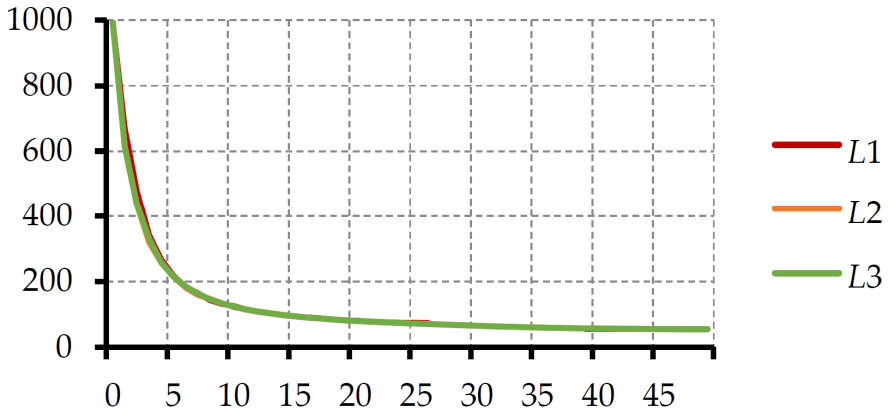

Figure 5. Temperature along the *L*1, *L*2, *L*3.

Orthogonal experiment is carried out to fit the simulated temperature field. As such, the temperature field on the rake face can be expressed as:

$$\begin{cases} T_r = P_1 e^{P_2\sqrt{x^2+y^2}} + (T_c - P_1)e^{P_3\sqrt{x^2+y^2}} \\ P_1 = 0.9546T_c - 14.5e^{-0.06356a_p} - 0.07785T_c a_p \\ P_2 = -6.208 + 18.46a_p - 24.92a_p^2 + 11.46a_p^3 \\ P_3 = -0.0103 - 0.02213T_c - 5.771 \times 10^{-5}a_p + 3.302 \times 10^{-5}T_c a_p \end{cases} \quad (3)$$

3.2.2. Temperature Filed on Main Flank Face

The temperature field on the main flank face is shown in Figure 6, where different colors represented the temperature distribution in the CFX simulation process. Following the above approach, the temperature field can be also approximately expressed via similar function models. Temperatures of the points located far away from the heat source are also assumed to be equal to the ambient temperature T_{air}. Therefore, the temperature field on the main flank face can be approximately expressed as:

$$\begin{cases} T_{f1} = P_1 e^{P_2\sqrt{x_1^2+y_1^2}} + (T_c - P_1)e^{P_3\sqrt{x_1^2+y_1^2}} \\ P_1 = 0.9224T_c - 10.26e^{-0.3025a_p} - 0.1566T_c a_p \\ P_2 = -8.004 + 28.41a_p - 46.52a_p^2 + 24.35a_p^3 \\ P_3 = -0.06248 - 0.04879T_c - 0.0001278a_p + 7.667 \times 10^{-5}T_c a_p \end{cases} \quad (4)$$

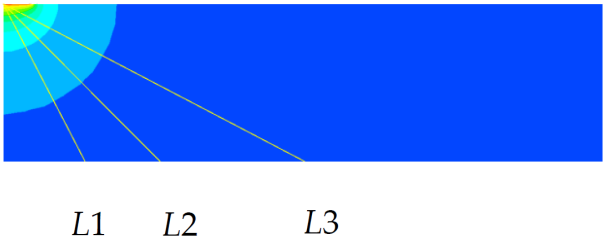

Figure 6. The simulated temperature field on the main flank face.

3.2.3. Temperature Filed on Minor Flank Face

Similar to the distribution of the temperature field on the rake face and that on the main flank face, the approximate fitting of the temperature field on the main flank face can also be summarized as:

$$\begin{cases} T_{f2} = P_1 e^{P_2\sqrt{x_2^2+y_2^2}} + (T_c - P_1)e^{P_3\sqrt{x_2^2+y_2^2}} \\ P_1 = 0.9199T_c - 8.931e^{-0.282a_p} - 0.1717T_c a_p \\ P_2 = -7.994 + 26.68a_p - 42.91a_p^2 + 22.23a_p^3 \\ P_3 = -0.06332 - 0.05758T_c - 0.0001317a_p + 7.637 \times 10^{-5} T_c a_p \end{cases} \quad (5)$$

3.3. Thermal Resistance Analysis

Two factors contribute significantly to the actual thermal resistance, that is, the equivalent thermal resistance between the channel and interface, and the contact resistance between the insert and the tool-holder.

3.3.1. Tool-Holder and Internal Fluid Channel

The proposed independent internal cooling structure, composed of connected cooling fluid channels, can be regarded as a novel form of cylindrical cooling systems (CCS). CCS is often theoretically characterized by temperature gradients in radial directions. As shown in Figure 7a, the cylindrical wall separates two fluids of different temperatures. According to Newton's law of heat transfer, the thermal resistance for radial conduction in a cylindrical wall is expressed as [16]:

$$R = \frac{\ln(r_2/r_1)}{2\pi Lk} \quad (6)$$

where r_1, r_2 are the radius of the inner surface and outer surface respectively; L is the length of the channel; and k is thermal conductivity.

We divide the interface surface between the insert and the tool-holder into different elements, as shown in Figure 7b. The connected internal fluid channels are located within the tool-holder and deployed according to the geometric shape of the tool-holder such that they are very closed to the interface marked by the blue dash lines in Figure 7b. The thermal resistance between the unit (i, j) can be regarded as the parallel connection of every internal fluid channel unit. Therefore, the thermal resistance of unit (i, j) is presented written as:

$$R_{(i,j)} = \frac{\prod_{k=1}^{n} R_{k,cylind}}{\sum_{k=1}^{n} R_{k,cylind}} \quad (7)$$

where $R_{k,cylind}$ is the thermal resistance between the kth internal fluid channel unit and unit (i, j) of the interface between the insert and the tool-holder, and n is the number of the unit.

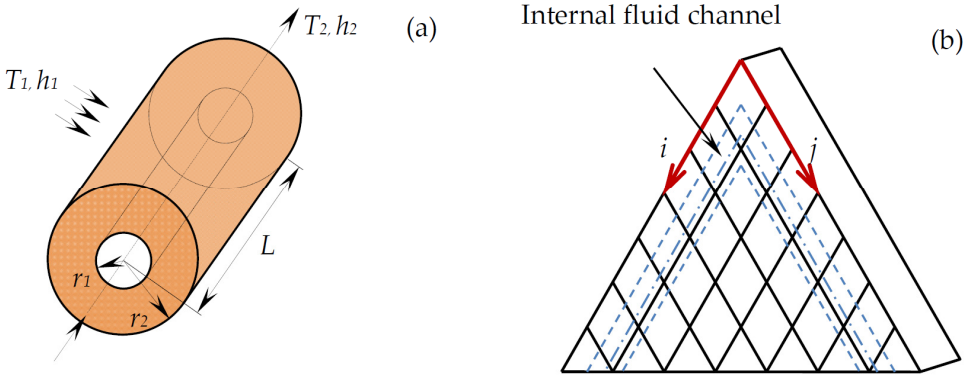

Figure 7. Schematic diagram of thermal resistance: (**a**) the cylindrical wall; (**b**) interface unit division.

From the above results, the thermal resistance distribution can be calculated to validate the enhancement of the heat transfer process. Figure 8 shows the thermal resistance at different locations on the interface in this research. A total of 840 points that are evenly spaced are sampled from the interface. Figure 8a is the coordinate definition diagram, with the origin located in the tool nose. The minimum thermal resistance located on the center of the interface indicates good heat dissipation performance in this interface.

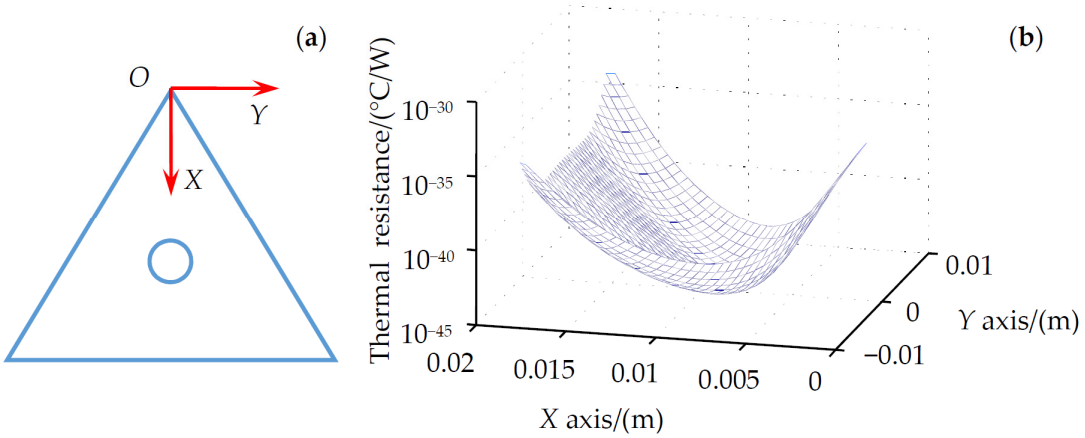

Figure 8. Thermal resistance: (**a**) Coordinate definition; (**b**) Thermal resistance distribution.

The Reynolds number is defined as the ratio between the inertia force and the viscous force [17,18], utilized to characterize different flow regimes within a similar fluid such as laminar or turbulent flow [19]. The Reynolds number is defined as:

$$R_e = \frac{UL}{v} = \frac{\rho v d}{\eta} \tag{8}$$

where U is a scale of variation of velocity in a length scale L; v is the velocity of flow; d is the diameter of the channel and η is the liquid viscosity. Therefore, the convection coefficient can be written as:

$$h_s = \lambda \frac{Nu}{l} = \lambda \frac{C {R_e}^m {P_r}^{1/3}}{l} \tag{9}$$

where λ represents the thermal conductivity of the fluid; $Nu = C{R_e}^m {P_r}^{1/3}$ is the Nusselt number [20]; the constants C and m can be chosen from references [20,21]; P_r is the Prandtl number; and l is the characteristic length.

The thermal circuit can be constructed on the basis of the fact that the thermal resistance is associated with the heat conduction between the insert and the tool-holder. The equivalent thermal resistance between the tool-holder and the internal fluid channel can be acquired as:

$$R_{ci} = \frac{1}{h_s A} + R_{cylind} \tag{10}$$

Therefore, on the interface between tool-holder and internal fluid channel, the heat flow can be expressed as:

$$q_{tl} = \frac{T_{insert} - T_o}{R_{ci}} \tag{11}$$

3.3.2. Interface between Insert and Tool-Holder

Owing to the existence of surface roughness, there is a temperature drop across the interface between the insert and the tool-holder. Generally, the associated contact resistance is influenced by the

roughness level of the mating surfaces and the joint pressure [16,22]. Treating insert and tool-holder as one-dimensional, the sketch is presented in Figure 9a.

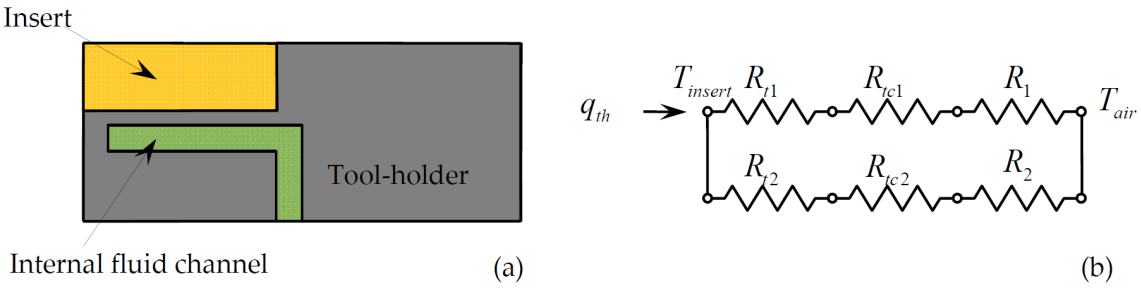

Figure 9. Insert and tool-holder (**a**) sketch; (**b**) thermal circuits.

The equivalent thermal resistance between the insert and the tool-holder can be regarded as the parallel circuits of the resistances through different directions (Figure 9b). Therefore, the equivalent thermal resistance is written as:

$$R_{th} = \frac{(R_{t1} + R_{tc1} + R_1)(R_{t2} + R_{tc2} + R_2)}{R_{t1} + R_{t2} + R_{tc1} + R_{tc2} + R_1 + R_2} \tag{12}$$

where R_{t1}, R_{t2}, R_1, R_2 are the thermal resistances associated with the process of heat conduction between the insert and the tool-holder. These quantities can be calculated using the formula $R = 1/(\lambda A_1/d + hA_2)$, where λ is the thermal conductivity, d is the thickness of a part, A_1 is the area of cross-section of a part, A_2 is the area of the surface exposed to the air, and h is the heat transfer coefficient of the area contact with air. R_{tc1}, R_{tc2} are the thermal contact resistance between the insert and the tool-holder and can be calculated using $R_{tc} = d/(\lambda_w A_w)$ where d is the thickness of the layer, A_w is the contact area, and λ_w is the thermal conductivity of water.

Therefore, on the interface between the insert and the tool-holder, the heat flow can be expressed as:

$$q_{th} = \frac{T_{insert} - T_{air}}{R_{th}} \tag{13}$$

3.4. Average Temperature of the Insert

T_{insert} is an indispensable parameter required by Equation (2), while the main focus in this research is the tool–chip interface. Therefore, it is significant to determine the instinct relationship. Dividing the insert into multiple small pieces from the different function faces, the average temperature of the insert can be regarded as the weighted mean temperature of these multiple small pieces. As such, the volume average temperature of the insert temperature can be written as:

$$\begin{aligned} T_{insert} &= \frac{\sum V_i T_i}{\sum V_i} \approx \frac{\sum A_i T_i}{\sum A_i} \\ &= \frac{AcTc + \iint_{A_r - A_c} T_r(x,y,t)dA + \iint_{A_{f1}} T_{f1}(x_1,y_1,t)dA + \iint_{A_{f2}} T_{f2}(x_2,y_2,t)dA + A_{tl}T_{tl} + A_{th}T_{th}}{\sum A_i} \end{aligned} \tag{14}$$

where A_i denote the area of different function faces.

3.5. Iterative Algorithm for Computing Cutting Temperature

On the basis of the above sub-sections, all the parameters in the energy equation shown in Equation (1) are explicitly specified. However, the derived equation is still very difficult to be evaluated analytically. Considering the available initial conditions given by $T_c(0) = T_{air}$ and $T_o(0) = T_i$, we employ numerical analysis techniques to solve the equation conveniently. The flowchart of the solving algorithm is presented in Figure 10.

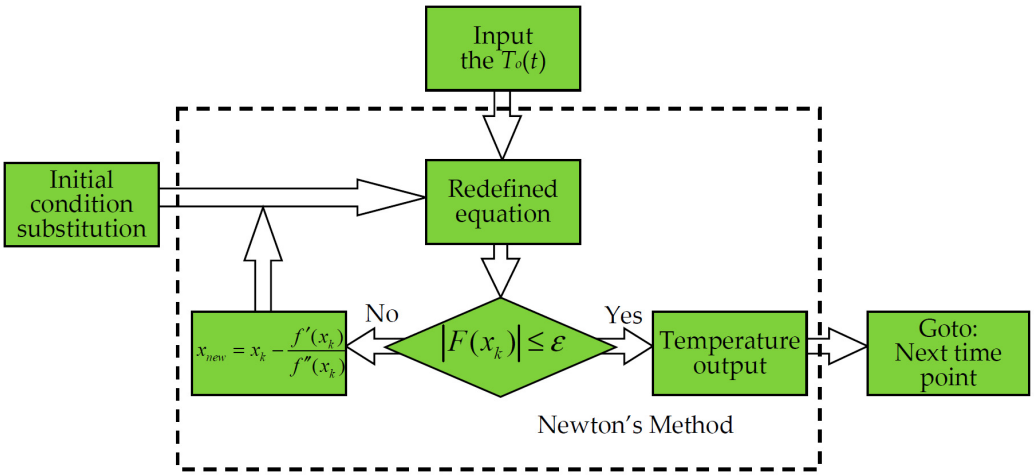

Figure 10. Temperature solving algorithm.

The numerical equation to be solved in the algorithm can be redefined as:

$$F(x) = c_t \rho_t V_t \frac{dT_{insert}}{dt} - qA_c q_r + q_{f1} + q_{f2} + q_{tl} + q_{th} \tag{15}$$

Initial values of the above equation are determined based on the empirical guess for the height of the tool–chip interface temperature. Substituting this temperature into the equation, new values of $F(x_k)$ are obtained. A tolerance error of a small value is allowed as the convergence criterion for the Newton's method [23]. The stopping criterion of the iterative algorithm is that $|F(x_k)| \le \varepsilon$, where ε is the numeric tolerance very close to zero, which controls the numerical accuracy as well as the convergence of the iterations. After evaluating all the temperature field in each iteration, the dynamical temporal evolution of the temperature field on the tool–chip interface, as well as its temperature field at specific time instance, are acquired conveniently.

3.6. Measure Point Temperature

As presented in Section 3.2, the temperature fields of these surfaces can also be calculated on the simulation platform of Ansys CFX.

3.6.1. Temperature Field along the Insert Thickness Direction

To fit the temperature field along the direction of insert thickness, a path of straight line is deployed to probe the temperatures. Owing to the comparatively consistent temperature distribution along the radial directions from the vertex of the interface, the path temperature along the insert thickness direction can be expressed as:

$$\begin{cases} y = ae^{bl} + ce^{dl} \\ a = 0.8718T_c - 37.062 \\ b = -1.698{a_p}^{-0.644} \\ c = 0.0882T_c + 32.495 \\ d = -0.3916e^{-2.72a_p} \end{cases} \tag{16}$$

where l is the distance between the measure point and the tool tip.

3.6.2. Temperature Field on the Interface of Insert and Tool-Holder

Figure 11 shows the temperature distribution of the interface of insert and tool-holder, where different colors represented the temperature distribution in the CFX simulation process.

The temperature distribution on the interface between the insert and the tool-holder can be expressed as:

$$\begin{cases} y = P_1\left(x^2+y^2\right)^{\frac{3}{2}} + P_2\left(x^2+y^2\right) + P_3\left(x^2+y^2\right)^{\frac{1}{2}} + t_{\max} \\ P_1 = 0.0001t_{\max} - 0.0004767e^{-11.62a_p} - 0.002207e^{0.1603a_p} \\ P_2 = \left(-0.0005202e^{-5.553a_p} - 0.00212e^{0.3082a_p}\right)t_{\max} + 0.03066e^{-19.73a_p} + 0.0449e^{0.244a_p} \\ P_3 = \left(-0.02449e^{-0.2466a_p} + 0.02115e^{-23.68a_p}\right)t_{\max} + 0.4889e^{-0.2458a_p} - 0.7004e^{-28.88a_p} \end{cases} \quad (17)$$

where $t_{\max}$ is the maximal temperature of the interface. Substituted the coordinate of measure point in Equation (17) the measure point temperature can be easy to acquire.

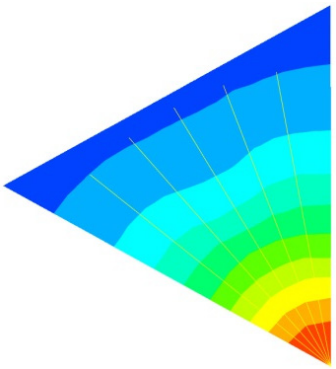

Figure 11. The temperature filed between the insert and tool-holder.

Based on the calculated temperature field on the tool-chip interface and the mathematical deductions illustrated above, temperatures of the three measure points can be acquired.

4. Numerical Analysis of the Thermal Performance

4.1. Description of the Experiment Setup

To investigate the heat transfer performance of the proposed internal cooling structure, a turning experiment was performed on a classical type of horizontal lathe. The type of the lathe is CA6236 and it is produced by the Shenyang machine tools company, Shenyang, Liaoning, China. The temperature field on the tool–chip interface was captured by an infrared thermal imager (Ti32, Fluke Corporation, Everett, WA, USA), and three thermocouples were used to measure the temperatures within the tiny grooves. An NI PXI data acquisition platform was utilized to measure the temperature. The sampling frequency was set as 80 Hz. The purified water was pumped with a peristaltic pump through the V-shaped channel and formed a closed internal cooling circuitry in the tool-holder. Considering the simplicity in this study, the coolant speed was kept constantly at 80 mL/min using a flowmeter. A workpiece in the form of hollow bar (the material is 1045 and its diameter is 60 mm) was chosen as the test specimen of the turning experiment. The machining parameters of the turning test are listed in Table 3. A photo of the experimental setup for turning trials is shown in Figure 12.

Table 3. Machining parameters of the turning test.

Parameter	Value
rotation speed of the spindle	410 r/min
feed speed	0.1 mm/r
cutting depth	1 mm

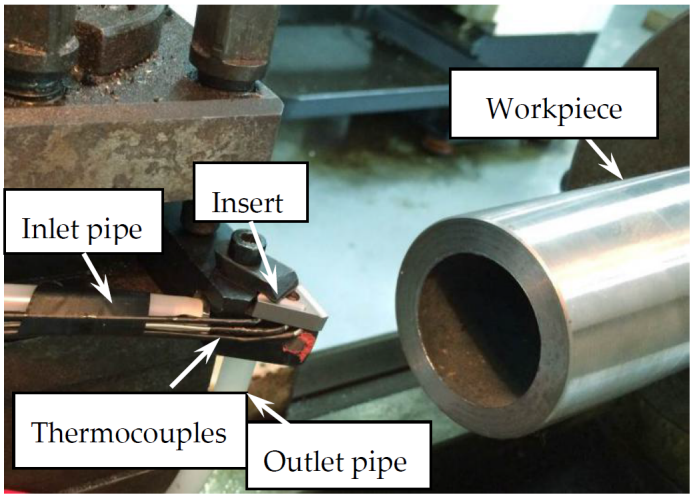

Figure 12. Photo of the experimental setup.

4.2. Experiment Data Processing and Analysis

Factors such as manufacturing error, deformation error, and electromagnetic interference (EMI) can be major error sources for the temperature measurement. Therefore, proper data post-processing is necessary for identify actual information from noisy observations. Proposed by Huang et al. [24], the technique of empirical mode decomposition (EMD) separates an original one-dimensional time domain signal into a number of oscillatory components named as intrinsic mode functions (*IMF*s). Furthermore, EMD also employs Hilbert transform to these *IMF*s such that meaningful information of instantaneous frequency and instantaneous amplitude can be revealed [25]. Based on the principles of EMD, a new type of mean filter is proposed to obtained smooth trend of the measurement and suppresses interfering noises.

Let $s(n)$ be the original one-dimension discrete series. EMD can be regarded as a mathematical tool characterized by the following representation [26]:

$$s(n) = \sum_{k=1}^{K} IMF_k(n) + r_{K+1}(n) \tag{18}$$

where $IMF_k(n)$ is the k-th oscillatory mode (or *IMF*) of the signal , and $r_{K+1}(n)$ is the residual trend (usually a component in the form of low-order polynomials).

Affected by actual environmental noises and the uncertainty of measurements, noisy contents were incorporated as interfering fluctuations occurred around the actual dynamic temperature curve in the measurement, shown in Figure 13a. The noisy fluctuations can be considered as high-frequency noises embedding in the low-frequency trend signal. Therefore, the original discrete signal $s(n)$ can be mathematically modeled as:

$$s(n) = \sum_{k=1}^{K} r_k(n) + LFS \tag{19}$$

where $r_k(n)$ is the k-th noise mode of the signal and *LFS* is the low-frequency component.

The procedure of EMD can be briefly summarized as searching the extremes of the data, connecting the entire local maximum via cubic spline curves as an upper envelope curve and a lower envelope curve [27,28]. As presented in Figure 13b, the enclosed area within the upper and the lower envelopes, marked by double dot dash lines, cover all the date samples between them. The instantaneous mean values can be evaluated as the trend line (Figure 13c). According to EMD, on condition that the resultant trend line does not satisfy the requirement, additional iterations named as the sifting process stated above is further conducted.

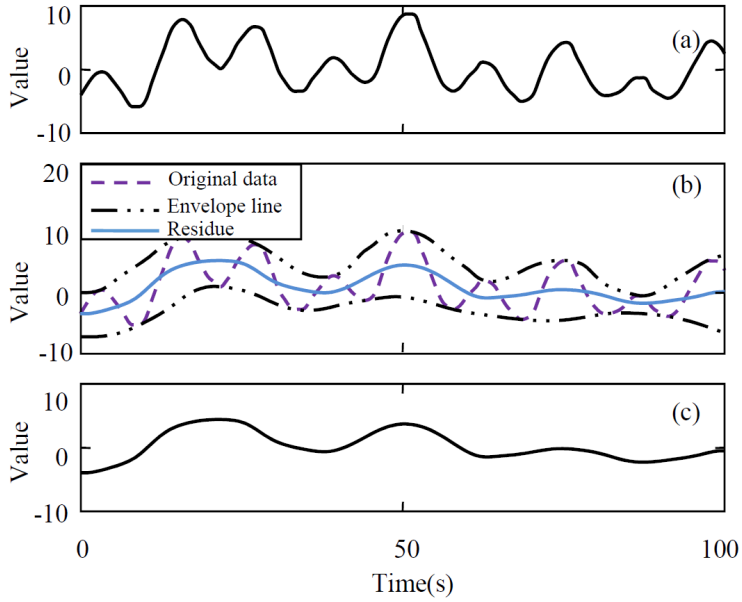

Figure 13. Filter principles of empirical mode decomposition (EMD). (**a**) The original data; (**b**) the envelope process; (**c**) the residue.

After performing post-processing, introduced as above, to the measured experimental data, temperatures of the measured points are presented in Figure 14. In Figure 14, the solid line is the first measure point nearest to the tool tip and the double dot dash line denotes the temperatures of the measure point of the greatest distance from the tool tip. The dimension of the horizontal axis indicates the time with a unit of second, while the dimension of the vertical axis indicates the temperature of the measure point with the unit of degrees Celsius. In Figure 14a, original curves demonstrating the temperatures of the specified points are displayed, from which it is remarkable that the high-frequency noises are so great that it is unable to distinguish the realistic temperatures of the points. In Figure 14b, the filtered data is shown. It is evident that the high-frequency noises have been substantially suppressed.

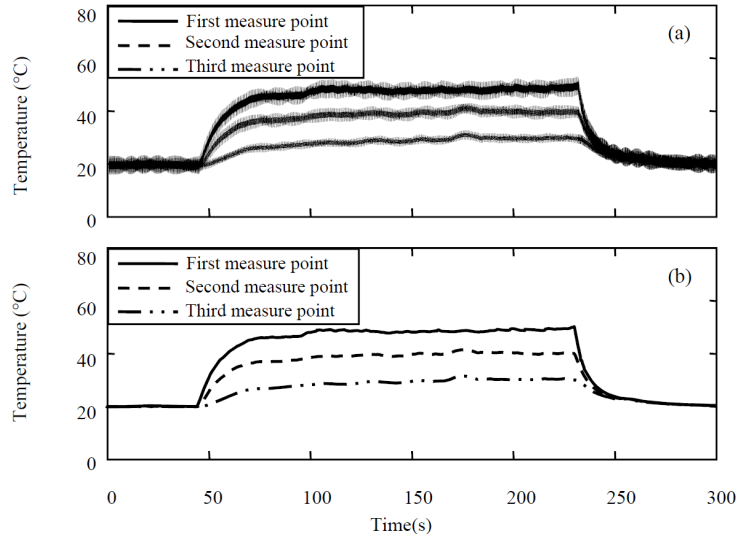

Figure 14. Filter result. (**a**) Measured temperature signal; (**b**) filtered temperature signal.

4.3. Temperature Comparison

According to the established model in Section 3, the dynamic temperature series of the tool—chip interface of the ascent stage is calculated and is shown in Figure 15. In Figure 15, the horizontal coordinate indicates the time with a unit of second; the vertical coordinate indicates the measure point with a unit of degree Celsius. As can be seen in this figure, the temperature of the interface increased to the highest temperature of 450 °C in 30 s and almost kept unchanged.

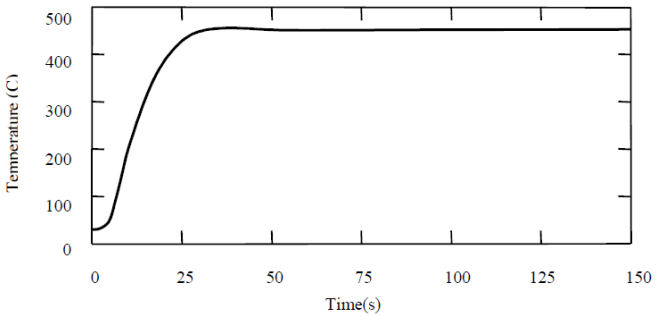

Figure 15. Predicted temperature on the tool–chip interface.

Tool–chip interface parameters are extremely difficult to estimate because of the high contact pressure, high temperature, and intense friction applied to the tool-chip interface during the machining process [29,30]. In this experiment, a thermal imager is employed to acquire the temperature. The measured temperature during the indirect cooling experiment is presented in Figure 16. Figure 16a is the captured tool–chip interface infrared image when the cutting temperature stays at the steady state. There is a reasonable error existing between the value of the actual maximal temperature (433.5 °C) and that of the predicted temperature (450 °C). As can be seen in Figure 16b, the temperature decreased dramatically with the insert leaving the workpiece, from 433.5 to 258.5 °C. Compared with Figure 15, the analytic results show a good consistence that indicates the rationality of established model.

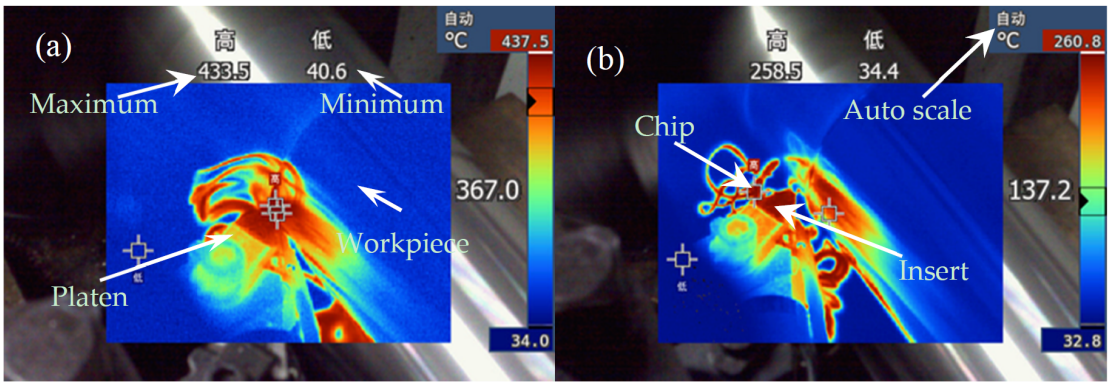

Figure 16. Captured infrared image of the tool-chip interface. (**a**) Steady machining state; (**b**) cutter-shaft backstroking process.

Figure 17 shows the measured temperature in the conventional dry cutting condition of the three measure points. Compared with Figure 14 which measured in the proposed indirect cooling system, the first measure point maximum temperature is decreased from 80.66 °C (dry cutting) to 58.47 °C (ICS), the second measure point maximum temperature was decreased from 69.94 °C (dry cutting) to 48.56 °C (ICS), and the third measure point maximum temperature was decreased from 59.23 °C (dry cutting) to 35.3 °C (ICS). These decreases indicate the feasibility and heat dissipation productiveness.

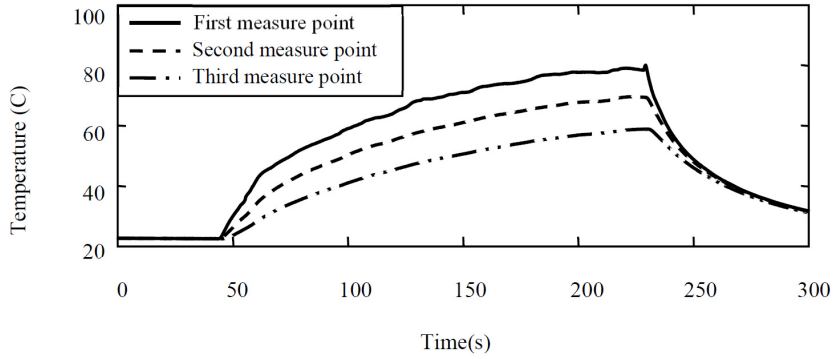

Figure 17. Temperature of the three measure points.

Figure 18 shows the temperature comparison between the experimental results (dotted dashed lines) and the numerical results (solid lines) of the placed three measure points the ascent stage. The comparisons show a good agreement which further support the validity of the proposed predicted models.

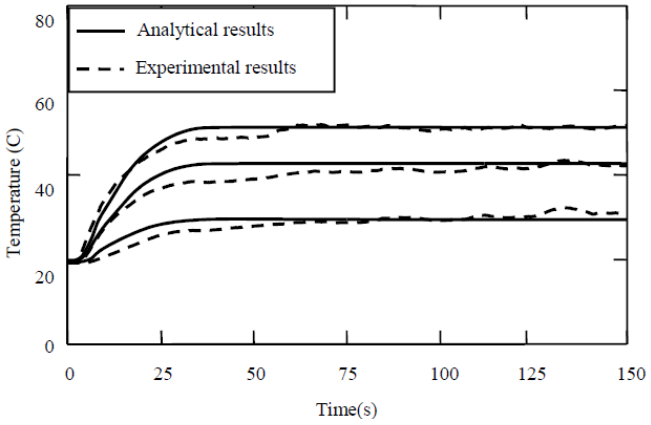

Figure 18. Comparison of the measure points.

5. Conclusions

In this paper, we proposed a novel independent internal cooling system. The novel type of ICS adopts closed internal fluid channels in the tool-holder for promoting heat dissipation during dry cutting processes. We derived the heat–energy balance equations of the insert system and Ansys CFX was employed to make numeric simulation of the actual temperature fields. The model of lumped parameter and Newton's iterative method were employed to solve the equation. A cutting trial on the lathe was presented to validate the established model and a new type of mean filter based on EMD was proposed to acquire the smooth signal. Major conclusions of this work can be summarized as below.

(1) The internal fluid channel could be utilized as an effective way to suppress excessive temperature rise on the tool–chip interface. Compared with conventional dry cutting, the maximal temperature on the measured point was decreased by almost 30% after using the internal fluid channel, independent of supplementary accessories.

(2) Results of the experimental with comparisons demonstrates that the measured temperature data are highly consistent with those of numerical simulations.

(3) The new type of mean filter, proposed based on principles of EMD, is very convenient for application to the data processing and has a remarkable suppressing ability for the high-frequency components.

According to the presented results, the proposed tool design and cooling solution can be also utilized for the machining of other materials. In the future, it would be worthwhile to investigate fluid of higher heat transfer coefficients on the independent cooling structure. Some other non-contact temperature measure methods are also worthy of further exploration.

Acknowledgments: This work was financially supported by the Natural Science Foundation of China (Grant No. 51605403), Fujian Provincial Industry-University-Research Cooperation Major Projects (Grant No. 2014H6025) and the Natural Science Foundation of Guangdong Province, China (Grant No. 2015A030310010).

Author Contributions: Bin Yao, Weifang Sun and Binqiang Chen conceived and designed the experiments; Xiaojin Yu and Yuchao He performed the experiment; Wei Feng analyzed the data; Shuyang Wang provided the experiment materials and the fixture design; Weifang Sun wrote the paper; Bin Yao and Binqiang Chen reviewed and edited the manuscript; all authors read and approved the manuscript.

Conflicts of Interest: The author declares no conflicts of interest.

References

1. Wu, Z.; Yang, Y.; Su, C.; Cai, X.; Luo, C. Development and prospect of cooling technology for dry cutting tools. *Int. J. Adv. Manuf. Technol.* **2017**, *88*, 1567–1577. [CrossRef]
2. Astakhov, V.P. *Tribology of Metal Cutting*; Elsevier: Amsterdam, The Netherlands, 2006.
3. Shokrani, A.; Dhokia, V.; Newman, S.T. Environmentally conscious machining of difficult-to-machine materials with regard to cutting fluids. *Int. J. Mach. Tools Manuf.* **2012**, *57*, 83–101. [CrossRef]
4. Rivero, A.; Aramendi, G.; Herranz, S.; De Lacalle, L.N.L. An experimental investigation of the effect of coatings and cutting parameters on the dry drilling performance of aluminium alloys. *Int. J. Adv. Manuf. Technol.* **2006**, *28*, 1–11. [CrossRef]
5. Haddag, H.; Nouari, M.; Kagnaya, T. A new heat transfer analysis in machining based on two steps of 3D finite element modelling and experimental validation. *Heat Mass Transf.* **2013**, *49*, 129–145. [CrossRef]
6. Haddag, B.; Atlati, S.; Nouari, M.; Zenasni, M. Analysis of the heat transfer at the tool–workpiece interface in machining: Determination of heat generation and heat transfer coefficients. *Heat Mass Transf.* **2015**, *51*, 1355–1370. [CrossRef]
7. Jerold, B.D.; Kumar, M.P. Machining of AISI 316 stainless steel under carbon dioxide cooling. *Mater. Manuf. Process.* **2012**, *27*, 1059–1065. [CrossRef]
8. Tazehkandi, A.H.; Shabgard, M.; Pilehvarian, F. Application of liquid nitrogen and spray mode of biodegradable vegetable cutting fluid with compressed air in order to reduce cutting fluid consumption in turning Inconel 740. *J. Clean. Prod.* **2015**, *108*, 90–103. [CrossRef]
9. Liang, L.; Quan, Y.; Ke, Z. Investigation of tool-chip interface temperature in dry turning assisted by heat pipe cooling. *Int. J. Adv. Manuf. Technol.* **2011**, *54*, 35–43. [CrossRef]
10. Chiou, R.Y.; Lu, L.; Chen, J.S.J.; North, M.T. Investigation of dry machining with embedded heat pipe cooling by finite element analysis and experiments. *Int. J. Adv. Manuf. Technol.* **2007**, *31*, 905–914. [CrossRef]
11. Ferri, C.; Minton, T.; Ghani, S.B.C.; Cheng, K. Internally cooled tools and cutting temperature in contamination-free machining. *Proc. Inst. Mech. Eng. C* **2014**, *228*, 135–145. [CrossRef]
12. Minton, T.; Ghani, S.; Sammler, F.; Bateman, R.; Fürstmann, P.; Roeder, M. Temperature of internally-cooled diamond-coated tools for dry-cutting titanium. *Int. J. Mach. Tools Manuf.* **2013**, *75*, 27–35. [CrossRef]
13. Sun, X.; Bateman, R.; Cheng, K.; Ghani, S.C. Design and analysis of an internally cooled smart cutting tool for dry cutting. *Proc. Inst. Mech. Eng. B* **2011**, *226*, 585–591. [CrossRef]
14. Shu, S.; Cheng, K.; Ding, H.; Chen, S. An innovative method to measure the cutting temperature in process by using an internally cooled smart cutting tool. *J. Manuf. Sci. Eng.* **2013**, *135*, 1247–1254. [CrossRef]
15. Shu, S.R. Design and Analysis of the Internally Cooled Smart Turning Tool and Experimental Study. Ph.D. Thesis, Harbin Institute of Technology, Harbin, China, 2014.
16. Incropera, F.P.; Dewitt, D.P.; Bergman, T.L.; Lavine, A.S. *Fundamentals of Heat and Mass Transfer*, 6th ed.; John Wiley & Sons: New York, NY, USA, 2007.
17. Kundu, P.K.; Cohen, I.M.; Dowling, D.R. *Fluid Mechanics*, 6th ed.; Elsevier: Amsterdam, The Netherlands, 2015.
18. Ding, Z.R. *Engineering Fluid Dynamics*; Machinery Industry Press: Beijing, China, 2013.
19. Sheikholeslami, M.; Ellahi, R. Electrohydrodynamic nanofluid hydrothermal treatment in an enclosure with sinusoidal upper wall. *Appl. Sci.* **2015**, *5*, 294–306. [CrossRef]

20. Hilpert, R. Heat transfer from cylinders. *Forsch. Geb. Ing.* **1933**, *4*, 215–224. [CrossRef]
21. Knudsen, J.G.; Katz, D.L.; Street, R.E. Fluid dynamics and heat transfer. *Phys. Today* **1958**, *12*, 40–44. [CrossRef]
22. Guillot, E.; Bourouga, B.; Garnier, B.; Dubar, L. Estimation of thermal contact parameters at a worpiece-tool interface in a HSM process. *Int. J. Mater. Form.* **2008**, *1*, 1031–1034. [CrossRef]
23. Leader, J.J. *Numerical Analysis and Scientific Computation*; Pearson: London, UK, 2004.
24. Huang, N.E.; Shen, Z.; Long, S.R.; Wu, M.C.; Shih, H.H.; Zheng, Q.; Yen, N.-C.; Tung, C.C.; Liu, H.H. The empirical mode decomposition and the hilbert spectrum for nonlinear and non-stationary time series analysis. *Proc. R. Soc. A* **1998**, *454*, 903–995. [CrossRef]
25. Rehman, N.U.; Mandic, D.P. Empirical mode decomposition for trivariate signals. *IEEE Trans. Signal Process.* **2010**, *58*, 1059–1068. [CrossRef]
26. Delechelle, E.; Lemoine, J.; Niang, O. Empirical mode decomposition: An analytical approach for sifting process. *IEEE Signal Process. Lett.* **2005**, *12*, 764–767. [CrossRef]
27. Zhou, Z.; Wu, W.; Wu, S.; Jia, K.; Tsui, P.-H. Empirical mode decomposition of ultrasound imaging for gain-independent measurement on tissue echogenicity: A feasibility study. *Appl. Sci.* **2017**, *7*, 324. [CrossRef]
28. Xu, J.; Wang, Z.; Tan, C.; Si, L.; Liu, X. A novel denoising method for an acoustic-based system through empirical mode decomposition and an improved fruit fly optimization algorithm. *Appl. Sci.* **2017**, *7*, 215. [CrossRef]
29. Haddag, B.; Nouari, M. Tool wear and heat transfer analyses in dry machining based on multi-steps numerical modelling and experimental validation. *Wear* **2013**, *302*, 1158–1170. [CrossRef]
30. Atlati, S.; Haddag, B.; Nouari, M.; Zenasni, M. Thermomechanical modelling of the tool–work material interface in machining and its implementation using the ABAQUS VUINTER subroutine. *Int. J. Mech. Sci.* **2014**, *87*, 102–117. [CrossRef]